Journal of Building Engineering 95 (2024) 110210

Contents lists available at ScienceDirect

Journal of Building Engineering

journal homepage: www.elsevier.com/locate/jobe

Topology optimization analysis of a frame-core tube structure using a cable-bracing-self-balanced inerter system

Liyu Xie [a], Zijian Yang [a], Songtao Xue [a,b], Ling Gong [a], Hesheng Tang [a,*]

[a] Department of Disaster Mitigation for Structures, Tongji University, Shanghai, China
[b] Department of Architecture, Tohoku Institute of Technology, Sendai, Japan

ARTICLE INFO

Keywords:
Cable-bracing-self-balanced inerter system
Outriggers
Modal control
Topology optimization

ABSTRACT

This paper describes the role of the cable-bracing-self-balanced inerter system (CBSBIS) for vibration control of frame-core tube structures and focuses on the efficiency improvements of the inerter system brought by the topology optimization corresponding to the cable-bracing schemes. Different cable-bracing schemes are proposed to explore the installation efficiency applied to frame-core tube structures. According to the characteristics of the bending deformation, the simplified discrete model of a frame-core tube structure with the CBSBIS is established, and an optimal design method based on the modal control is proposed from the perspective of the convenience of design. According to the results of parameter analysis and numerical cases, the vertical bracing scheme is more effective in utilizing the overall bending deformation of the frame-core tube structure, particularly through the outriggers, which amplify the displacement driving the CBSBIS. Meanwhile, the damping effect of controlling multiple modes of the structure is demonstrably superior to that of controlling a single mode. Compared with the traditional damped outrigger and tuned mass damper, the CBSBIS provide a better solution for the control of structures which means that the CBSBIS has a significant improvement in the control of the structure's harmful inter-story drift ratio and acceleration response.

1. Introduction

The main problem faced when designing super high-rise buildings is that the building becomes more sensitive to lateral forces as the height increases. The frame-core tube structure is the most used type of super high-rise buildings. The outrigger connects the core tube and the perimeter columns to improve the lateral resistance of the structure [1,2]. Some researchers have further improved the ability of frame-core tube structure to resist lateral loads by optimizing the position of the outriggers [3–5]. However, the traditional outrigger truss cannot improve the structural damping, which is beneficial to energy dissipation during a dynamic load. Studies showed that most of tall buildings over 250 m have a level of an inherent damping ratio of less than 1 % [6,7]. Some researchers have installed viscous dampers between the outriggers and perimeter columns which are called damped outriggers (DO) to improve structural damping energy dissipation [8–11]. But the maximum achievable damping ratio of the damper outrigger structure is influenced by the stiffness ratio of core tube to perimeter columns. The stiffness ratio is recommended to be less than 3.7 to achieve a 5 % damping ratio [12,13]. It is difficult to achieve a satisfactory damping ratio by adding a damped outrigger for a perimeter column with limited stiffness. Das et al. [14,15] proposed a shape memory alloy (SMA) based damped outrigger and verified its better

* Corresponding author.
E-mail address: thstj@tongji.edu.cn (H. Tang).

https://doi.org/10.1016/j.jobe.2024.110210
Received 11 January 2024; Received in revised form 10 July 2024; Accepted 12 July 2024
Available online 14 July 2024

performance in controlling the dynamic response of the structure under seismic excitation compared to viscous damper-based outrigger system. Wang et al. [16,17] developed a negative stiffness damped outrigger (NSDO) by combining negative stiffness elements to amplify the damping effect. Compared with the conventional damped outrigger (CDO), the NSDO significantly improves the modal damping ratio. Wang et al. [18] conducted a comparative study of CDO, NSDO, and their combined use under random excitation and demonstrated that the combination of NSDO and DO provides superior results. Nevertheless, NSDO is only effective in improving the modal damping of the structure in the first few orders. Furthermore, negative stiffness devices are often achieved by releasing the elastic potential energy of the pre-compressed spring. Therefore, when static deformation occurs, it is difficult to reset the device to its equilibrium position due to the lack of restoring force, which leads to a continuous reduction of the elastic potential energy and a significant reduction in effectiveness.

Similar to NSDO, the inerter system also plays a role in damping enhancement. In the meanwhile, it can also benefit from the tuned mass damper's (TMD) dynamic energy absorption, which is superior for reducing structural vibration [19–21]. The inerter is a two-terminal mass element which means that its output force is directly proportional to the disparity in acceleration between its two terminals. Based on the analogy between mechanical and electrical networks, Smith [22] first termed this two-terminal inertial element as inerter and proposes a rack and pinion inerter. Inerter system is a novel passive control system that combines inerter elements, spring elements, and damping elements to coordinate their work for vibration control. Compared with some traditional passive vibration control methods, many researchers have demonstrated that the inerter system can produce an apparent mass far greater than its actual physical mass and can also enhance the energy dissipation effect of the damper by increasing the working stroke of the damper. In the field of civil engineering, Ikago [23–27]team combined the tuned spring and viscous mass damper for the first time and proposed the tuned viscous mass damper (TVMD) system which uses the ball screw to achieve a mass amplification mechanism. The topological forms and potential applications of the inerter system have also been researched and broadened on the basis of the TVMD's proposal. In 2014, Lazar et al. [28]proposed an inertia-based device called tuned inertia damper (TID), which parallels the damping element with the spring element and then connects them in series with the inerter element. In the subsequent research [29], it has been demonstrated that the TID has a better vibration reduction control effect than the classical viscous damper (VD). During the same year, based on the application of inerter and the generalization of TMD system Marian et al. [30] proposed the tuned mass damper inerter (TMDI) and verify its better performance under random excitation compared to TMD. The TVMD, TID and TMDI are the three most widely used topologies for inerter systems in civil engineering [31–39]. In order to study different series-parallel topology forms, Pan and Zhang et al. [40] matched the inerter element with those of the damping element and the spring element to achieve better control. In addition to building structures, the utilization of inerter-based control systems is becoming increasingly prevalent in a diverse range of applications, including wind turbines [41,42], cables [29,35], automotive suspensions [43,44], spacecraft [45] and energy harvesting [46].

Similarly, many scholars have done research on the optimization of mechanical parameters of inerter systems. Saito et al. [24] gave a parameter optimization method for the TVMD system based on fixed-point theory optimization method which represents a class of H_∞ optimization schemes for regulating the peaks of structural frequency response functions [47]. Pan and Zhang [48,49] proposed an optimization design method based on performance requirements, which is essentially an H_2 optimization approach based on structural frequency response functions. In addition to optimization methods derived from the frequency domain, there are also metaheuristic algorithms [36,38,50] for multi-objectives which perform a large number of iterative calculations through the certain rule designs to obtain the optimization parameters.

Although the research on inerter systems has been relatively mature, this innovative passive control system is less used in high-rise buildings. On the one hand, most studies use inter-story relative displacement to drive inerter system. However, high-rise structures show different deformation properties than shear structures, so the installation schemes should be reconsidered. For instance, Fig. 1 depicts the typical configuration of dampers in bending and shear structures. It is clear that the damper layout for a shear structure primarily takes into account the fact that its energy consumption depends on the horizontal relative displacement of the structure, whereas the damper layout for a bending structure relies on the rotation of the structural floor to produce the outermost tension and compression deformation. Of course, some researchers have also shown the way to install inerter systems in high-rise buildings. The two main connection schemes are shown in Fig. 2. The first installation scheme mainly uses the bending deformation of the structure to drive inerter system and realize the vibration control of the structure by connecting the inerter system with the outrigger. Asia and Ikago [51,52] proposed for the first time to apply the inerter system between the outrigger and the perimeter column of a high-rise bending structure. The second way is to use the inter-story relative displacement for inerter system. Xie et al. [32,53,54] achieved

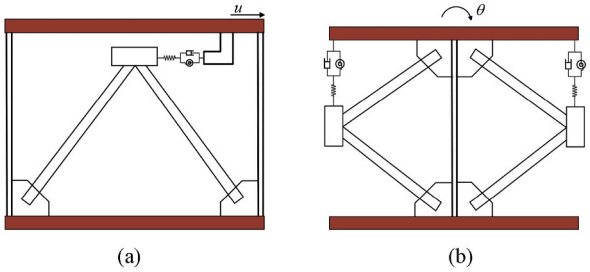

Fig. 1. Common structural damper installation methods (a) Damper arrangement of shear structure; (b) Damper arrangement of bending structure.

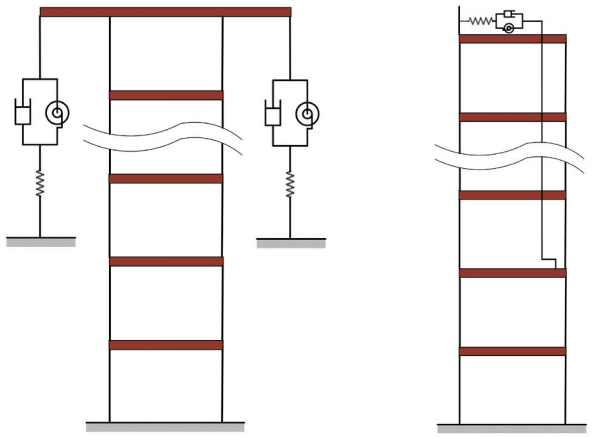

Fig. 2. Common connection schemes for inerter systems (a) Outrigger connection scheme; (b) Cross-layer connection scheme.

the accumulation of inter-story displacements to drive the damping control system through the cable arrangement across the layers. However, the small relative inter-story displacements of high-rise bending structures cannot fulfil the energy dissipation role of the inerter system. In practice, the cross-story connection way dominates, so inter-story displacements can be accumulated.

On the other hand, the bracing of the inerter system in the high-rise building is required to have a certain deformation capacity and stability regardless of the installation schemes shown in Fig. 2. When the installation span is considerable, the conventional rigid connection way is prone to buckling and has poor shape adaptation. Currently, one method for achieving the self-resetting energy dissipation system support is to use the pure tension system of the central energy dissipation member and the cable. The combination of the cable and the compression material can solve the compression buckling problem of the support member and is easy to install. Pekcan et al. [55] proposed a damping cable system. The system is simple to install, taking full advantage of the benefits of the cable support system, and eliminating the impact of buckling under the conventional connection schemes by connecting the damper to the main structure with cables. Hou et al. [56] first proposed a method of seismic strengthening of steel frames using wire cable bracing, demonstrating its effectiveness as a support member for vibration control under large displacements. Gao et al. [57] applied a cross-braced connection form of tension cables to form a lateral force-resisting system, illustrating the re-centred and energy-dissipating effects of a pure tension system. Asadi et al. [58] conducted experimental and numerical simulations to verify that the use of shape-memory alloy wires to connect the damper can achieve an increase in its equivalent damping ratio and self-centring function. Lee et al. [59] experimentally verified the effectiveness of tension-only shape-memory alloy device for steel moment-resisting frames under seismic excitation. Kang et al. [60] proposed a vibration control system for seesaw structures based on fluid viscous dampers, using pure tension support members connected to the structure, and demonstrated that a seesaw energy dissipation system under a pure tension system could effectively control the response of the structure. In order to use an inerter system in a pure tension system, it is primarily necessary for it to have the ability to self-reset or self-balance in the condition of double endpoint output. Xie et al. [32,53,54] proposed a new type of inerter system connected by cables, called cable-bracing inerter system (CBIS). The adaptable benefits of CBIS include simple installation and suitability for discontinuous floor layouts. Xie designs the parameters of the inerter system by single-objective and multi-objective optimization approaches and verify its damping effect. However, the study of CBIS is still limited to shear structures, without considering the application in structures dominated by bending deformation.

Based on the idea of energy dissipation of the damped outrigger, this paper uses the outrigger as the connection to explore the effect of the cable-bracing-self-balanced inerter system (CBSBIS) on the vibration control of the frame-core tube structure and investigates the effectiveness of different cable-bracing schemes in utilizing structural rotation angle and cumulative inter-story displacements in the high-rise bending structure. Additionally, a method based on modal control is proposed as an easy-to-design solution. Finally, the effectiveness of CBSBIS topology optimization and modal control is verified by numerical examples.

2. Detail of CBSBIS

2.1. A self-balanced inerter system

Fig. 3 shows a schematic diagram of a self-balanced inerter system. The damping element is connected in parallel with the inerter and then in series with the stiffness element. Specifically for this paper, a ball screw type inerter has been adopted which converts the translational motion of the screw into the high-speed rotation of the flywheel to achieve the effect of apparent mass amplification. Eddy current damping in parallel with the inerter is achieved by mounting a back iron plate, conductor plate and permanent magnets on the flywheel. The stiffness of the system is achieved by a combination of springs in series with pre-stressed cables. Given that the stiffness of the cable cannot be infinite, it is reasonable to consider the additional stiffness brought about by the series connection of the cable and the spring in the actual engineering design. Additionally, it is essential to apply an appropriate prestressing to the cable in advance to prevent the cable from relaxing as a consequence of the loss of displacement transfer. The output of inerter system can be

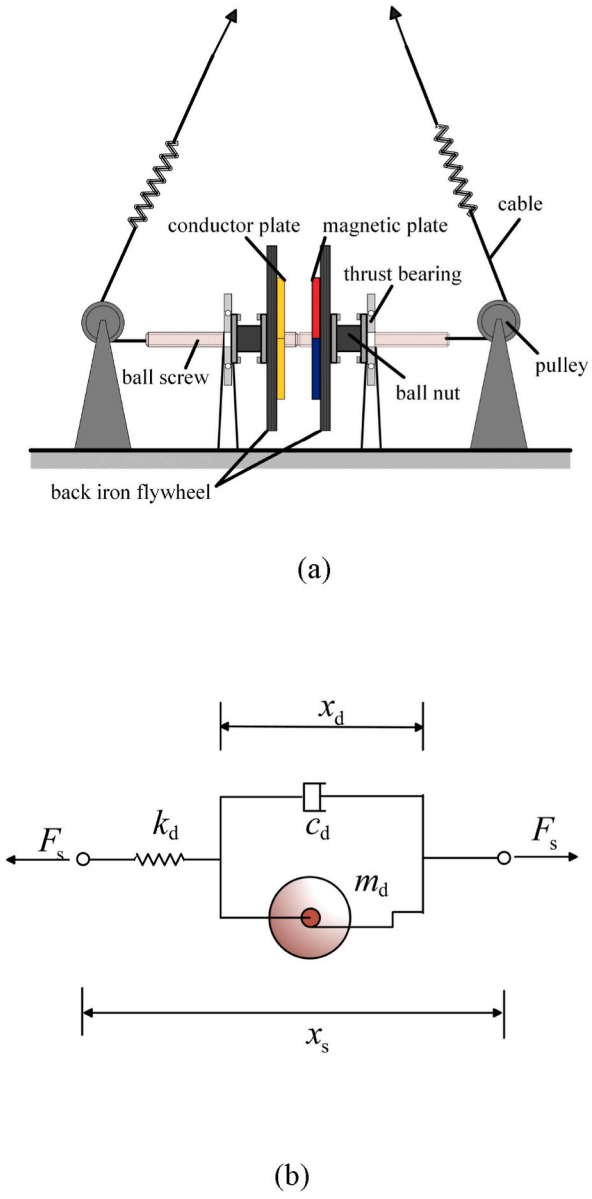

Fig. 3. Self-balanced inerter system (a) Device diagram; (b) Simplified mechanical model.

expressed as:

$$F_s = k_d(x_s - x_d) = m_d\ddot{x}_d + c_d\dot{x}_d \tag{1}$$

Where x_d and x_s are the displacements of the inerter system and the structure, respectively; the corresponding displacement is shown in Fig. 3b; m_d is the apparent mass of the inerter; k_d is the stiffness of the tuning spring, and c_d is the damping coefficient of the damping energy dissipation element.

A more detailed diagram of the self-balanced inerter is shown in Fig. 4. The screw rod with right-hand and left-hand threads are the key to achieving self-balanced inerter. When the screw rod moves in the axial direction, the symmetrical flywheels in different thread directions rotate in opposite directions, balancing the torque applied to the screw rod. This counterbalance relieves the torque constraints required at the end of the screw rod to allow a purely tensile cable connection which facilitates the simplification of the installation of the device. At the same time the apparent mass m_d of the self-balanced inerter is determined by Eq. (2).

$$m_d = m_0\left(r_0^2 + r_d^2\right)\left(\frac{2\pi}{l_d}\right)^2 \tag{2}$$

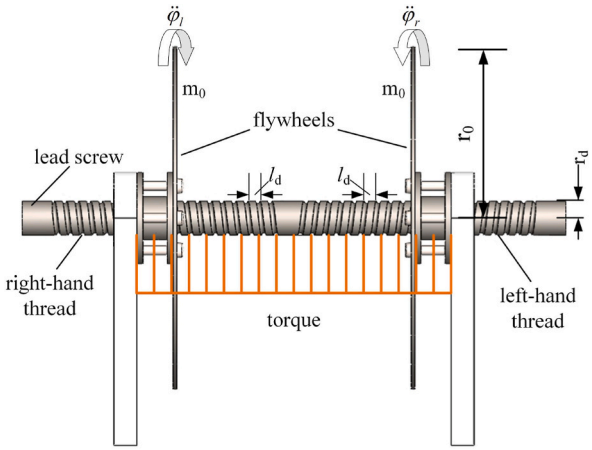

Fig. 4. Self-balanced inerter.

where m_0 is the mass of the flywheel, r_0 and r_d are the radius of the flywheel and screw rod, respectively, and l_d is the lead of the ball screw. The rational design of r_0 and l_d enables the amplification of the flywheel's mass by a factor of thousands.

2.2. Different schemes of cable-bracing

In the frame-core tube structure, the CBSBIS is fixed to the outrigger truss through the cable to play the role of vibration control. The control performance of the device is dependent on different installation strategies of the cables. As shown in Fig. 5, three topological forms of cable are proposed in this research based on the deformation properties of the frame-core tube structures. The first scheme is the vertical connection, in which the cables are attached vertically to the outrigger to drive the inerter system by structural rotational deformation and the outrigger can amplify the rotational deformation effect of the structure. The second scheme uses an inverted-V connection, where the cables are fixed in the center of the core to take advantage of the cumulative relative inter-story displacement of the structure. The third way is the diagonal cable bracing, in which the cable is fixed diagonally to the outrigger on the opposite side. This method utilizes both the cumulative relative interlayer displacement and the rotational deformation of the structure, combining the characteristics of the first two connection schemes.

In the real structure, the stiffness of the outrigger truss is quite large, therefore to simplify the analysis in this paper, its bending stiffness and shear stiffness are assumed to be infinite. The following analyses investigate the displacement transfer relationship between the outrigger truss and the inerter system with different installation strategies of the cables.

The diagonal cable is driven by the joint action of horizontal displacement and rotation. It is reasonable to assume that the cable movements are independent of being driven by the structure's rotation and horizontal displacement if the structure falls into the category of small deformation during vibration. So, the final result can be obtained by linear superposition. The relationship between structural displacement and cable displacement is shown in Fig. 6.

The simplified relationship between cable displacement x_c and structural displacement x and rotation angle θ can be obtained as follows:

$$x_c = x\cos\alpha - \frac{l\sin\alpha}{2}\theta \tag{3}$$

In the case of inverted-V cable bracing scheme, the rotation angle of the structure has no effect on the displacement of the inerter system. Therefore, the relationship between the cable displacement and the structural displacement is shown in Fig. 7.

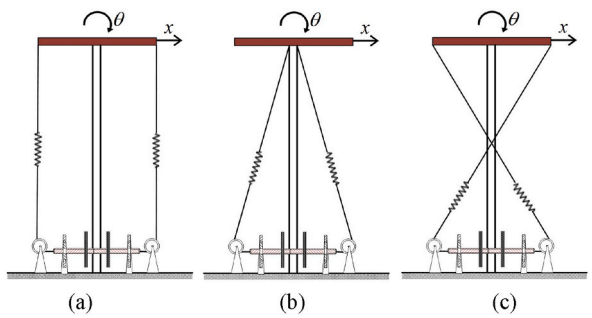

Fig. 5. Schematic diagram of three cable bracing forms (a) Vertical cable bracing; (b) Inverted-V cable bracing; (c) Diagonal cable bracing.

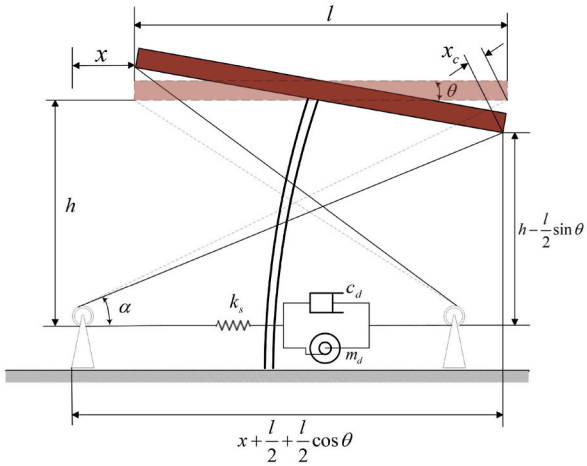

Fig. 6. Deformation diagram of diagonal cable bracing.

The relationship between the displacement of the simplified cable and the structural displacement can be obtained as follows:

$$x_c = x\cos\alpha \tag{4}$$

In the case of vertical cable bracing, only the influence of the structure's rotation on the cable displacement is taken into consideration because the horizontal movement of the cables on both sides is the same, meaning that the horizontal displacement of the structure has no effect on the inerter system.

According to the geometric relationship in Fig. 8, the relationship between structural displacement and cable displacement in the case of vertical cable bracing scheme can be expressed as:

$$x_c = \frac{l}{2}\theta \tag{5}$$

Based on the above three connection schemes, the relationship between cable displacement and structural displacement can be uniformly expressed as the relationship between lateral displacement and rotation of the structure. It can be considered that the cable inclination angle α and the total length of outrigger l determine the corresponding coefficients. The relationship between simplified cable displacement and structural displacement can be expressed as:

$$x_c = \beta_x x + \beta_\theta \theta \tag{6}$$

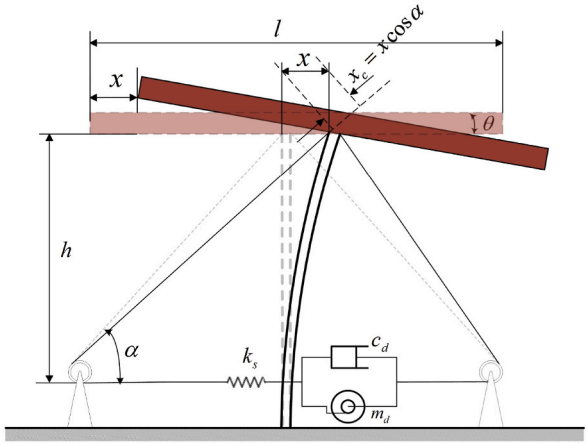

Fig. 7. Deformation diagram of inverted-V cable bracing.

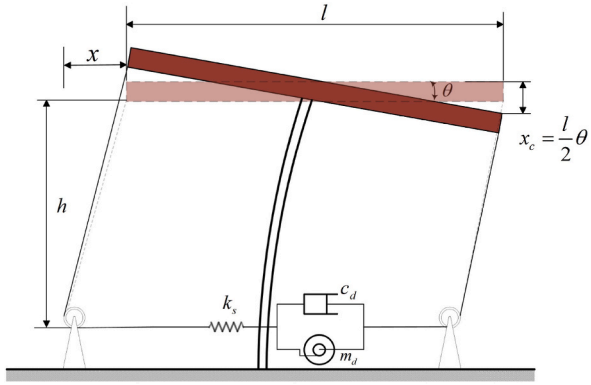

Fig. 8. Deformation diagram of vertical cable bracing.

$$\begin{cases} \beta_x = \cos\alpha, \beta_\theta = 0 & \text{Inverted} - \text{V cable bracing} \\ \beta_x = 0, \beta_\theta = \dfrac{l}{2} & \text{Vertical cable bracing} \\ \beta_x = \cos\alpha, \beta_\theta = -\dfrac{l}{2}\sin\alpha & \text{Diagonal cable bracing} \end{cases} \tag{7}$$

It can be seen from Eq. (7) that the length of the outrigger is proportional to the contribution of the inerter system driven by the structural rotation angle. The outrigger amplifies the rotation effects of the structure which means that the displacement of the cable fixed to the outrigger truss is greater for the same angle of rotation.

3. Modelling and analysis of the frame-core tube structure with a CBSBIS

3.1. Government equations of the frame-core tube structure with a CBSBIS

For the frame-core structures, the main load-bearing members consist of the core tube and perimeter columns connected by outrigger. To simplify subsequent dynamic analysis, this paper assumes that the core and perimeter columns form a unified flexural system, and the ends of the outrigger trusses are used as anchorages for the cable. This assumption is reasonable because the core and perimeter columns satisfy the condition of deformation coordination under the constraint of the extension truss. A forty-storey frame-core tube structure and its corresponding simplified discrete model proposed by Gamaliel [61] are used as illustrative structures in this paper to investigate the vibration reduction performance of CBSBIS with different topological forms. Each lumped mass contains two degrees of freedom: one in the translational direction and one in the rotational direction. The degrees of freedom in the vertical direction are neglected due to the relatively small deformation. Figs. 9 and 10 show the real structure and the simplified discrete model, respectively. The equations of motion for the simplified model subjected to the ground acceleration $\ddot{x}_g$ can be expressed as follows:

$$M_m\ddot{x}_m + C_m\dot{x}_m + K_m x_m = -M_m r_m \ddot{x}_g \tag{8}$$

where M_m is the mass of the main structure, C_m is the damping matrix and K_m is the stiffness matrix. The mass matrix is a diagonal matrix containing the mass and rotational inertia of the floor, expressed as follows:

$$M_m = diag\{\, m_1 \quad J_1 \quad m_2 \quad J_2 \quad \cdots \quad m_n \quad J_n \,\} \tag{9}$$

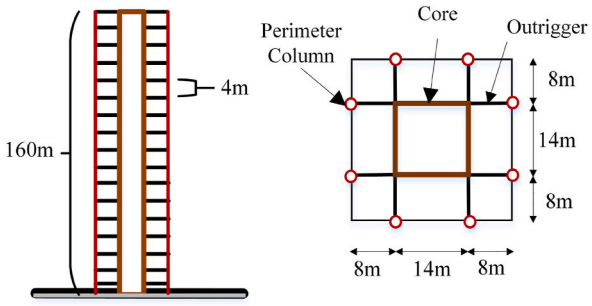

Fig. 9. Schematic diagram of a forty-story frame-core tube structure.

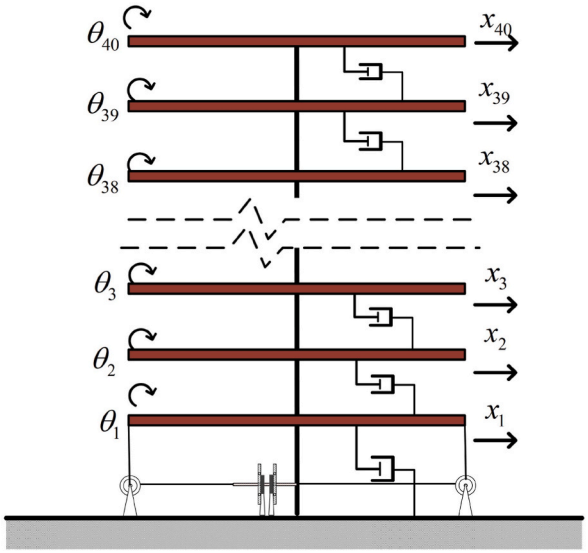

Fig. 10. Schematic of a simplified discrete model.

Where m_i and J_i are the ith layer's mass, rotational inertia; n represents the number of degrees of freedom of the model, which is consistent with the number of floors. The rotational inertia is assumed to be provided by the concrete core only.

The Rayleigh damping assumption is adopted in the damping matrix. x_m is the displacement and rotation of each floor of the structure as Eq. (10); r_m is the seismic force action vector as Eq. (11).

$$x_m = [x_1, \theta_1, x_2, \theta_2, \cdots, x_n, \theta_n]^T \tag{10}$$

$$r_m = [1, 0, 1, 0 \cdots, 1, 0]^T \tag{11}$$

The connection unit between each lumped mass is modelled as a Euler-Bernoulli beam unit, and the stiffness matrix K_m obtained is as Eq. (12), where A is the area of the core; E is elastic modulus of the core; I is the moment of inertia of the core with respect to the bending axis; L is the floor height and α is the angle of reference with respect to the global coordinate

The initial three orders of the vibration modes of the structure are obtained using a simplified discrete model as shown in Fig. 11. The results are consistent with the bending deformation of the frame-core tube structure.

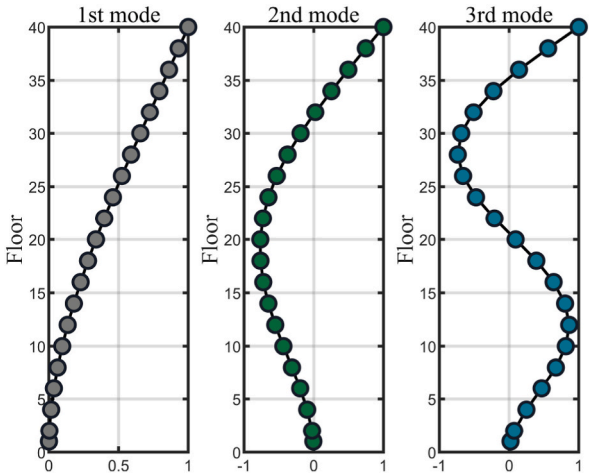

Fig. 11. Schematic of the vibration model.

$$K_{\mathrm{m}}=\begin{bmatrix} k_{1\mathrm{bb}}+k_{1\mathrm{aa}} & k_{1\mathrm{ab}} & & & & \\ k_{1\mathrm{ab}} & k_{1\mathrm{bb}}+k_{2\mathrm{aa}} & k_{2\mathrm{ab}} & & 0 & \\ & k_{2\mathrm{ba}} & k_{2\mathrm{bb}}+k_{3\mathrm{aa}} & & & \\ & & & \ddots & k_{(\mathrm{n}-2)\mathrm{ab}} & \\ & 0 & & k_{(\mathrm{n}-2)\mathrm{ba}} & k_{(\mathrm{n}-2)\mathrm{bb}}+k_{(\mathrm{n}-1)\mathrm{aa}} & k_{(\mathrm{n}-1)\mathrm{ab}} \\ & & & & k_{(\mathrm{n}-1)\mathrm{ba}} & k_{(\mathrm{n}-1)\mathrm{bb}}+k_{(\mathrm{n})\mathrm{aa}} \end{bmatrix} \tag{12}$$

$$\begin{cases} k_{(i)\mathrm{aa}}=\begin{bmatrix} \frac{AE}{L}\sin^2\alpha+\frac{12EI}{L^3}\cos^2\alpha & \frac{6EI}{L^2}\cos\alpha \\ \frac{6EI}{L^2}\cos\alpha & \frac{4EI}{L} \end{bmatrix} & k_{(i)\mathrm{ba}}=\begin{bmatrix} -\frac{AE}{L}\sin^2\alpha+\frac{12EI}{L^3}\cos^2\alpha & \frac{6EI}{L^2}\cos\alpha \\ -\frac{6EI}{L^2}\cos\alpha & \frac{2EI}{L} \end{bmatrix} \\ k_{(i)\mathrm{ab}}=\begin{bmatrix} -\frac{AE}{L}\sin^2\alpha+\frac{12EI}{L^3}\cos^2\alpha & -\frac{6EI}{L^2}\cos\alpha \\ \frac{6EI}{L^2}\cos\alpha & \frac{2EI}{L} \end{bmatrix} & k_{(i)\mathrm{bb}}=\begin{bmatrix} \frac{AE}{L}\sin^2\alpha+\frac{12EI}{L^3}\cos^2\alpha & -\frac{6EI}{L^2}\cos\alpha \\ -\frac{6EI}{L^2}\cos\alpha & \frac{4EI}{L} \end{bmatrix} \end{cases} \tag{13}$$

The cables are selected to be anchored at every fourth floor of the structure, due to the existence of reinforcement. Fig. 12 shows the different layouts of the CBSBIS in structure. It is important to note that the cables be anchored across floors, thus the building layout, for example elevator shafts, pipelines, etc., can be utilised effectively in the actual installation to reduce the installation openings. The equations of motion for frame-core structures equipped with the CBSBIS are as follows:

$$M\ddot{x}+C\dot{x}+Kx=-Mr\ddot{x}_{\mathrm{g}} \tag{14}$$

$$\begin{cases} x=\left[x_{\mathrm{m}}{}^{T},x_{\mathrm{d}}\right]^{T} \\ r=\left[r_{\mathrm{m}}{}^{T},0\right]^{T} \\ M=\begin{bmatrix} M_{\mathrm{m}} & 0 \\ 0 & m_{\mathrm{d}} \end{bmatrix} \\ C=\begin{bmatrix} C_{\mathrm{m}} & 0 \\ 0 & c_{\mathrm{d}} \end{bmatrix} \\ K=\begin{bmatrix} K_{\mathrm{m}}+T_{\mathrm{c}}^{\mathrm{T}}k_{\mathrm{d}}T_{\mathrm{c}} & -T_{\mathrm{c}}^{\mathrm{T}}k_{\mathrm{d}} \\ k_{\mathrm{d}}T_{\mathrm{c}} & k_{\mathrm{d}} \end{bmatrix} \end{cases} \tag{15}$$

where m_{d} , c_{d} and k_{d} are apparent mass, damping coefficient and tuning stiffness of the CBSBIS respectively; x_{d} is the displacement of inerter; T_{c} is the transformation matrix of the cable displacement, depending on the scheme of cable-bracing, inerter system installation and anchorage position. When the CBSBIS is installed in $i_{\mathrm{d}}{}^{\mathrm{th}}$ layer and the cables are anchored in $j_{\mathrm{d}}{}^{\mathrm{th}}$ layer, the expression for T_{c} is as follows:

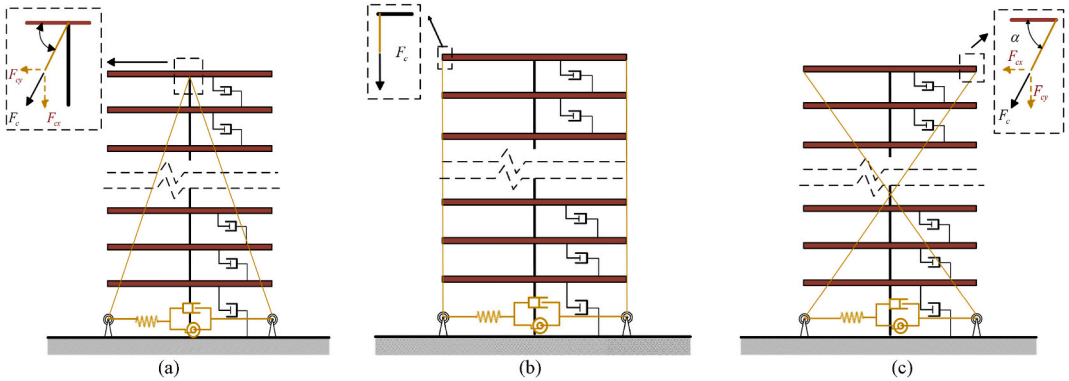

Fig. 12. Schematic of different cable-bracing schemes in the frame-core tube structure.

$$\begin{cases} T_c = \beta_x R_{cx} + \beta_0 R_{c\theta} \\ R_{cx} = R_{c\theta} = \left[\underbrace{0,\cdots,\overbrace{-1}^{i_d},\cdots,\overbrace{1}^{j_d},0,\cdots,0}_{2n}\right] \text{(ungrounded)} \\ R_{cx} = R_{c\theta} = \left[\underbrace{0,\cdots,\overbrace{1}^{j_d},0,\cdots,0}_{2n}\right] \text{(grounded)} \end{cases} \tag{16}$$

3.2. Parameter optimization for modal control

Ikago et al. [24] derive an expression for the optimization parameters of an inerter system applied to a single degree of freedom structure using fixed point theory. For multi-degree-of-freedom structures, the effective control band of the inerter system is narrow due to the characteristics of the linear control system. Therefore, this paper adopts the strategy of controlling specific modes of the structure to enhance the performance of CBSBIS and simplify its design. The modal decomposition of Eq. (8) is shown below:

$$\phi_i{}^T M_m \phi_i \ddot{q}_{mi} + \phi_i{}^T C_m \phi_i \dot{q}_{mi} + \phi_i{}^T K_m \phi_i q_{m_i} = -\phi_i{}^T M_m r_m \ddot{x}_g \tag{17}$$

where ϕ_i is the i^{th} order vibration mode of the structure and q_{mi} is the corresponding generalized coordinate. Assuming that the structure vibrates in a specific mode, the displacements of the structure and the inerter can be expressed by the previous derivation as follows:

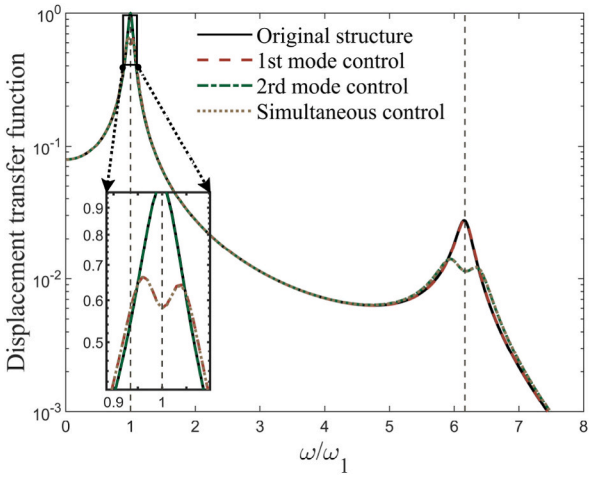

Fig. 13. The displacement transfer function of the top floor of the structure(a) displacement; (b) acceleration.

$$\begin{cases} x_{\mathrm{m}} = \phi_i q_{\mathrm{m}i} \\ x_{\mathrm{d}} = T_{\mathrm{c}} \phi_i q_{\mathrm{d}i} \end{cases} \tag{18}$$

By substituting Eq. (18) into Eq. (14), the following equations of motion are obtained with respect to the generalized coordinates $q_{\mathrm{m}i}$ and $q_{\mathrm{d}i}$.

$$\begin{cases} \overline{m}\ddot{q}_{\mathrm{m}i} + \overline{c}\dot{q}_{\mathrm{m}i} + \overline{k}q_{\mathrm{m}i} + \overline{k}_{\mathrm{d}}(q_{\mathrm{m}i} - q_{\mathrm{d}i}) = -{\phi_i}^{T} M_{\mathrm{m}} r_{\mathrm{m}} \ddot{x}_{\mathrm{g}} \\ \overline{m}_{\mathrm{d}}\ddot{q}_{\mathrm{d}i} + \overline{c}_{\mathrm{d}}\dot{q}_{\mathrm{d}i} + \overline{k}_{\mathrm{d}}(q_{\mathrm{d}i} - q_{\mathrm{m}i}) = 0 \\ \overline{m} = {\phi_i}^{\mathrm{T}} M_{\mathrm{m}} \phi_i, \overline{m}_{\mathrm{d}} = {\phi_i}^{\mathrm{T}} T_{\mathrm{c}}^{\mathrm{T}} m_{\mathrm{d}} T_{\mathrm{c}} \phi_i \\ \overline{c} = {\phi_i}^{\mathrm{T}} C_{\mathrm{m}} \phi_i, \overline{c}_{\mathrm{d}} = {\phi_i}^{\mathrm{T}} T_{\mathrm{c}}^{\mathrm{T}} c_{\mathrm{d}} T_{\mathrm{c}} \phi_i \\ \overline{k} = {\phi_i}^{\mathrm{T}} K_{\mathrm{m}} \phi_i, \overline{k}_{\mathrm{d}} = {\phi_i}^{\mathrm{T}} T_{\mathrm{c}}^{\mathrm{T}} k_{\mathrm{d}} T_{\mathrm{c}} \phi_i \end{cases} \tag{19}$$

The modal generalized mass ratio μ_i can be defined on the basis of the above equation as follows:

$$\mu_i = \frac{\overline{m}_{\mathrm{d}}}{\overline{m}} = \frac{{\phi_i}^{\mathrm{T}} T_{\mathrm{c}}^{\mathrm{T}} m_{\mathrm{d}} T_{\mathrm{c}} \phi_i}{{\phi_i}^{\mathrm{T}} M_{\mathrm{m}} \phi_i} \tag{20}$$

Comparing Eq. (19) and the equations of motion of a single degree of freedom structure equipped with inerter system [24], it can be obtained that the optimization parameters of the inerter system for the i^{th} order modal control of a multi-degree-of-freedom structure using the fixed-point theory as follows:

$$\begin{cases} {m_{\mathrm{d}}}^{\mathrm{opt}} = \dfrac{\mu_i {\phi_i}^{\mathrm{T}} M_{\mathrm{m}} \phi_i}{{\phi_i}^{\mathrm{T}} T_{\mathrm{c}}^{\mathrm{T}} T_{\mathrm{c}} \phi_i} \\ {k_{\mathrm{d}}}^{\mathrm{opt}} = \dfrac{\mu_i {\phi_i}^{\mathrm{T}} K_{\mathrm{m}} \phi_i}{(1-\mu_i) {\phi_i}^{\mathrm{T}} T_{\mathrm{c}}^{\mathrm{T}} T_{\mathrm{c}} \phi_i} \\ {c_{\mathrm{d}}}^{\mathrm{opt}} = \mu_i \sqrt{\dfrac{3\mu_i}{(1-\mu_i)(2-\mu_i)}} \dfrac{{\phi_i}^{\mathrm{T}} M_{\mathrm{m}} \phi_i}{{\phi_i}^{\mathrm{T}} T_{\mathrm{c}}^{\mathrm{T}} T_{\mathrm{c}} \phi_i} \omega_i \end{cases} \tag{21}$$

Where ω_i is the i^{th} order natural frequency of the structure. Generally, a larger mass ratio provides better control of the i^{th} order modes of the structure, but the corresponding cost is higher and this has to be weighed against the choice. Because of the superposition of linear systems, multiple CBSBIS can be installed to control multiple modes of the structure at the same time.

The effect of controlling the first and second order modes of the structure separately and simultaneously is demonstrated below using the displacement transfer function of the structure as an example of the vertical cable bracing. The inerter system is installed on the ground floor and the cable is anchored on the top floor. The corresponding optimization parameters of the inerter system are obtained according to Eq. (21) in the table below. Fig. 13 shows the displacement transfer function for the horizontal displacement of the top floor of the structure.

Fig. 13a and b demonstrate that the CBSBIS installed for structure-specific modal control has a favourable effect on the corresponding peak modal responses of both the top layer displacement and acceleration and has little influence on the other modes. Therefore, it can be seen that simultaneous control of the first and second order modes of the structure can effectively reduce the peak resonance response

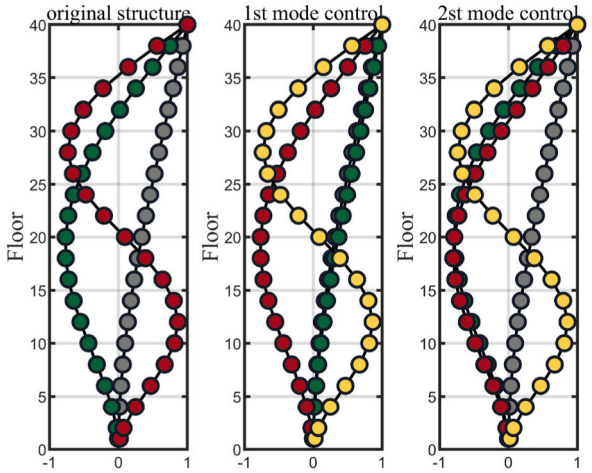

Fig. 14. Vibration shapes of the original structure and structure equipped with the CBSBIS.

corresponding to the first and second order modes at the same time. The reasons for the low mutual influence of the modal control are as follows: i, due to the different natural frequencies of each order of the structure, the CBSBIS needs to be tuned to optimise different frequencies resulting in a weaker effect on the control of the other modes; ii, from the discussion in the following sections, it is clear that the optimal installation location of the CBSBIS for the control of the different modes is different, resulting in a further weakening of the effect on the other modes. Fig. 14 illustrates the first three orders of vibration shape of the original structure and the first four orders of vibration shape of the structure with CBSBIS installed to control the structure for the first two orders of modes of the structure, respectively. It can be observed that for structure-specific mode control, the installation of CBSBIS adds a mode to the structure, with the mode shapes and self-oscillation frequencies essentially remaining consistent with those of the original structure, without affecting other modes. This is consistent with the frequency response function of the structure depicted in Fig. 13. This effectively reduces the peak response of the modes to be controlled without significantly affecting the dynamic behaviour of the structure.

3.3. Topology optimization for modal control

The cable displacement transformation matrix T_c has a significant impact on the control performance of the CBSBIS, as demonstrated in the previous sections. It is determined mainly by the installation schemes and the anchorage position of the cable. Therefore, this section focuses on the optimized installation position and schemes of the CBSBIS for the example frame-core tube structure.

From the modal control method in the previous section, it is known that the modal generalized mass ratio μ_i determines the control effect of the equivalent two-degree-of-freedom system shown in Eq. (19). The relationship between the modal generalized mass ratio and the optimized CBSBIS mechanical parameters is obtained through Eq. (21). It is evident that for a certain modal generalized mass ratio, the larger the $T_c\phi_i$, the smaller the mechanical parameters required, indicating the higher the control efficiency of the system. To quantify the effect of topology optimization of the CBSBIS, the modal displacement transformation efficiency coefficient β_i is defined as follows:

$$\beta_i = T_c\phi_i \tag{22}$$

The larger the β_i, the more efficient the CBSBIS is, theoretically, in controlling the specific modes of the structure. Although in practice the cables are anchored to the reinforcing layer of the example structure, the CBSBIS can be installed at any floor to better demonstrate the effect of different installation positions on the β_i. Figs. 14 and 15 show the variation of normalized β_i for different cable-bracing schemes and all possible anchorage positions for first and second order modal control of the structure.

Fig. 15 shows that the optimal anchorage location for the first order modal control of the structure is the top layer with the largest deformation. Additionally, the vertical cable-bracing scheme is more suitable for the bending deformation predominantly frame-core tube structure, compared to the diagonal and inverted-V cable-bracing schemes that utilize shear deformation predominantly. Fig. 16 shows the optimal anchorage location for the second order modal control of the structure. The vertical connection remains the most effective for the frame-core tube structure. It can be observed that the optimal installation position of CBSBIS has substantially changed and that the various connection schemes of the cable result in different optimal installation positions. It is also clear that for inappropriate installation positions for higher order modal control of the structure, β_i is close to zero, which can lead to very poor control performance of the CBSBIS. Consequently, it is of paramount importance to select the installation position of CBSBIS for the control of different modes of the structure. Table 2 lists the optimal installation locations for different cable-bracing schemes for the first second order modal control of the structure. The first value in brackets represents the level at which the inerter is located (0 for ground level) and the last value represents the level at which the cable is anchored.

Fig. 17 displays the displacement and acceleration transfer functions for different positions of the CBSBIS installed with the optimized parameters for first-order modal control given in Table 1. It can be seen that the optimum installation position has the best control of the resonance peak for the first mode, whereas CBSBIS has almost no effect when the cables are anchored in the bottom where the underlying deformation is small.

3.4. Parameter analysis for CBSBIS

This section focuses on the transfer function to investigate the effect of CBSBIS parameter variations on the resonance peaks corresponding to each mode. Eq. (19) provides the equations of motion for the equivalent two-degree-of-freedom system

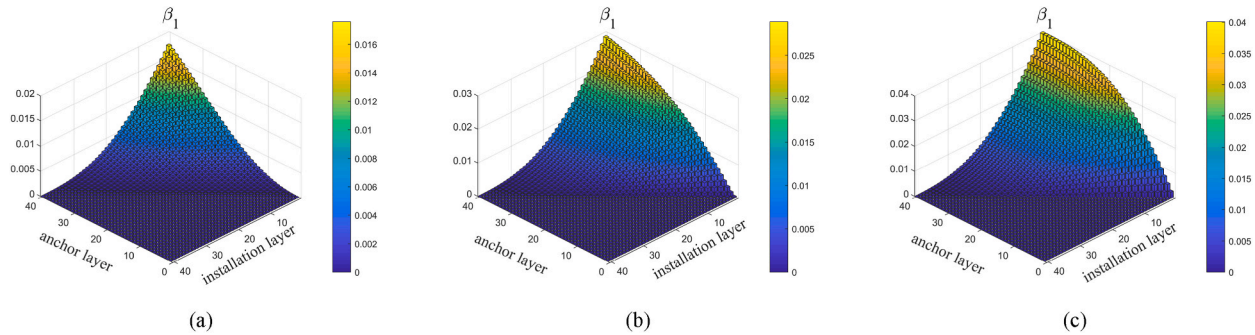

Fig. 15. Schematic diagram of first order modal control with different anchorage positions for beta(a) Diagonal cable bracing; (b) Inverted-V cable bracing; (c) Vertical cable bracing.

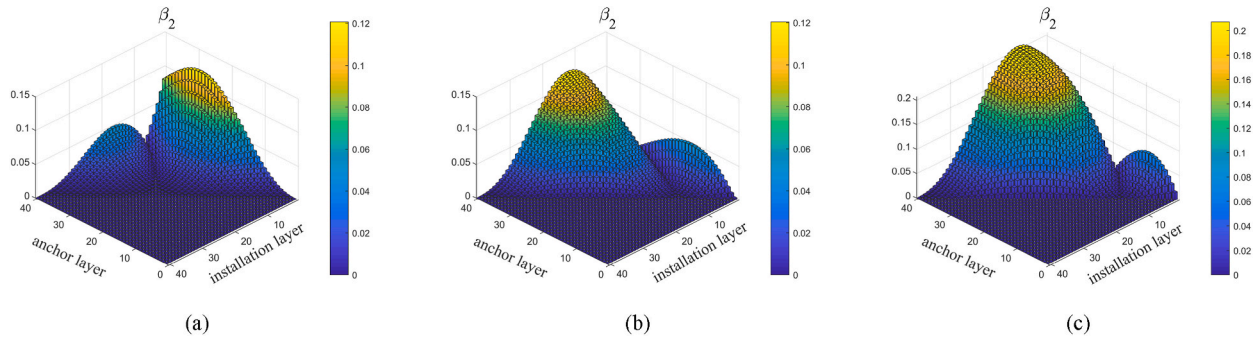

Fig. 16. Schematic diagram of second order modal control with different anchorage positions for beta(a) Diagonal cable bracing; (b) Inverted-V cable bracing; (c) Vertical cable bracing.

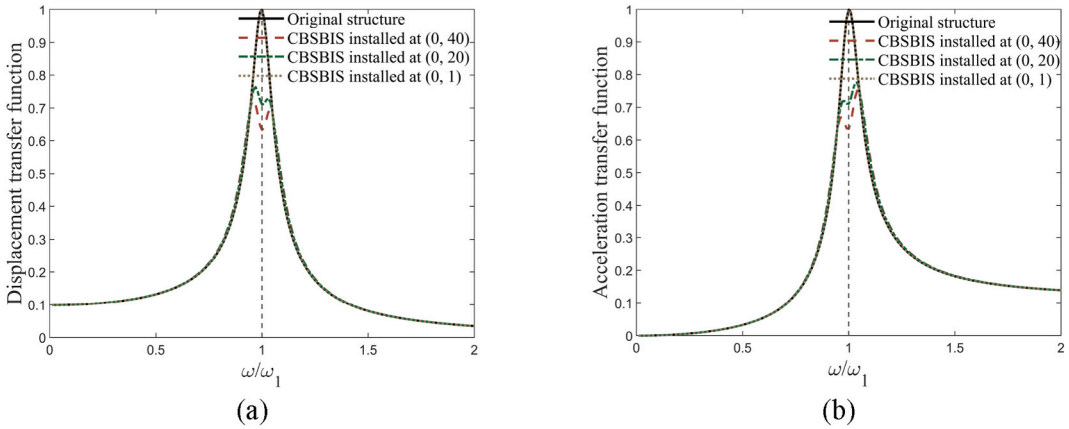

Fig. 17. The transfer function of the top floor of the structure for different anchorage position (a) displacement; (b) acceleration.

Table 1
Optimal parameters by fixed-point theory.

modes to be controlled	μ_i	m_d^{opt} (10^5kg)	c_d^{opt} (10^2 kN/m/s)	k_d^{opt} (10^3 kN/m)
1	0.005	6.534	1.356	3.740
2	0.005	0.553	0.708	12.036

Table 2
Modal control of optimal anchorage position.

cable-bracing scheme	1st mode	2st mode
Diagonal cable bracing	(0,40)	(12,40)
Inverted-V cable bracing	(0,40)	(0,29)
Vertical cable bracing	(0,40)	(9,40)

corresponding to each order of modes of the structure. It is evident that the control effect of CBSBIS on the equivalent system corresponds to the control effect on the relevant modes of the structure. Eq. (19) is dimensionlessised as follows:

$$\begin{cases} \ddot{q}_{mi} + 2\zeta_i\omega_i\dot{q}_{mi} + \omega_i{}^2 q_{mi} + \kappa_i\omega_i{}^2(q_{mi} - q_{di}) = a_{0i} \\ \mu_i\ddot{q}_{di} + 2\xi_i\omega_i\ddot{q}_{di} = \kappa_i\omega_i{}^2(q_{mi} - q_{di}) \end{cases} \tag{23}$$

$$\begin{cases} \omega_i = \sqrt{\dfrac{\phi_i{}^T K_m \phi}{\phi_i{}^T M_m \phi_i}}, \zeta_i = \dfrac{\phi_i{}^T C_m \phi_i}{2\omega_i \phi_i{}^T M_m \phi_i}, a_{0i} = \dfrac{-\phi_i{}^T M_m r_m \ddot{x}_g}{\phi_i{}^T M_m \phi_i} \\ \kappa_i = \dfrac{\phi_i{}^T T_c^T k_d T_c \phi_i}{\phi_i{}^T K_m \phi_i}, \xi_i = \dfrac{\phi_i{}^T T_c^T c_d T_c \phi_i}{2\omega_i \phi_i{}^T M_m \phi_i} \end{cases} \tag{24}$$

By Laplace transform on both sides of the above formula, defining $\beta = \omega/\omega_i$, the transfer function of corresponding generalized coordinate q_{mi} can be obtained as follows:

$$H(i\beta) = \frac{L(q_{mi})}{\omega_i{}^2 L(a_{0i})} = \frac{-\mu_i\beta^2 + 2\beta\xi_i i + \kappa_i}{2\zeta_i\beta\left(\beta^2\mu_i i - \kappa_i i + 2\beta\xi_i\right) + 2\xi_i\beta i\left(\beta^2 - \kappa_i - 1\right) + \beta^2\kappa_i\mu_i - \left(1-\beta^2\right)\left(\kappa_i - \mu_i\beta^2\right)} \tag{25}$$

The research in this paper is concerned with the control of the peak response of each mode of the structure. In order to calculate the maximum displacement response of the structure, define the norm H_∞ as:

$$H_\infty = \max\{|H(i\beta)|\} \tag{26}$$

Figs. 18 and 19 illustrate the impact of variations in CBSBIS's stiffness and damping on the peak displacement response of the first and second modal equivalent system of the structure. The CBSBIS is installed in a vertical cable-bracing way and in an optimal position. The modal generalized mass ratio μ_i is 0.05, 0.1, and 0.2, respectively, and the generalized stiffness ratio κ_i and generalized damping ratio ξ_i are [0.01, 0.5], and [0.001, 0.1], respectively. As can be seen in Figs. 18 and 19, there is a valley in the peak displacement response in the parameter domain, and the parameters optimized by modal control lie exactly within this valley. Furthermore, an increase in the modal generalized mass ratio results in a decrease in the peak displacement response. In addition, the dashed line in Fig. 18 indicates the range of parameter values where the peak response of the structure after installation of CBSBIS is reduced by 70 % relative to the original frequency domain peak response of the structure. It can be seen that the parameters obtained from the modal control optimization are still well within this range and allow for some parameter variation. This means that even with some variation in the CBSBIS tuning, there is still good vibration control performance. This confirms the validity and robustness of the parameter optimization formulation for modal control proposed in the previous section.

3.5. Design flowchart of CBSBIS

Based on the previous discussions of CBSBIS topology optimization and structural modal control methods, the design flow of CBSBIS as shown in Fig. 20 can be summarized as follows.

Step 1: *Initial structural analysis and identification of modes to be controlled.* It should be noted that CBSBIS can also be applied to other structural types. In this paper, the frame-core tube structure is chosen as the research object because its overall bending deformation characteristics and the existence of outrigger are more conducive to the discussion and effect enhancement of different topological forms of CBSBIS. The initial structural analysis is conducted with the objective of obtaining the dynamic properties of the structure, which serve as the foundation for subsequent topology optimization and modal control. The modes to be controlled are identified by analyzing the contribution of each mode to the dynamic response of the structure.

Step 2: *Calculate the modal displacement transformation efficiency coefficient β and determine the connection scheme and installation location of the CBSBIS.* This step calculates the modal displacement transformation efficiency coefficient β for the different cable connection scheme and installation positions of the CBSBIS for the modes to be controlled. The coefficient β reflects the efficiency of the different topological forms of the CBSBIS to utilize the structural deformation to drive itself into action. The optimal cable arrangement and installation position of the CBSBIS is thus obtained by maximizing the coefficient. It should be noted that in the context of a specific project, the installation of the CBSBIS should be considered in conjunction with the architectural layout of the structure. This involves the use of lift shafts, pipe shafts and other existing channels to arrange the cable in a way that avoids the later openings and other destructive layout.

Step 3: *Design optimization parameters for CBSBIS.* This step is concerned with the determination of the parameters of CBSBIS through the modal control parameter optimization method. It should be noted that following the determination of the parameters, the cable anchor nodes must be reinforced by the prediction of the output force in order to prevent damage.

Step 4: *Validation.* It is necessary to verify that the dynamic response control of the structure equipped with CBSBIS achieves the target performance. If this is not met, it is necessary to return to step 1 to increase the number of modes of the structure to be controlled or to return to step 3 to increase the design mass ratio.

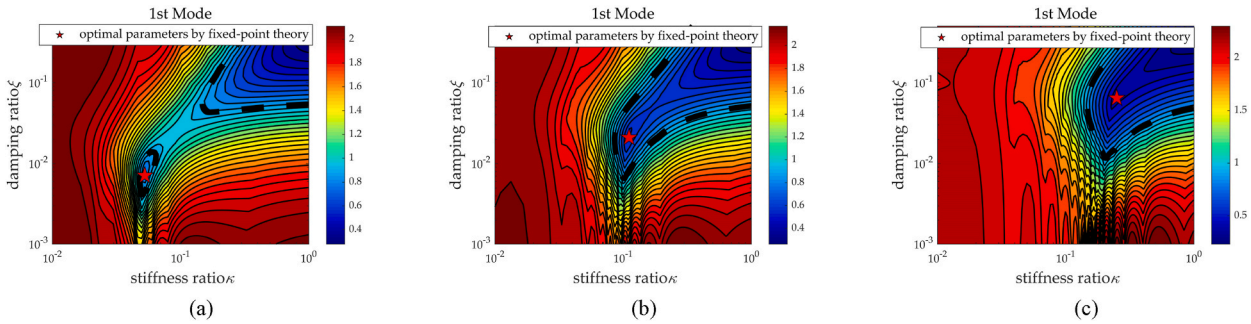

Fig. 18. Contour plots of the maximum displacement response of the structural first mode equivalent system(a) $\mu = 0.05$;(b) $\mu = 0.10$;(c) $\mu = 0.20$.

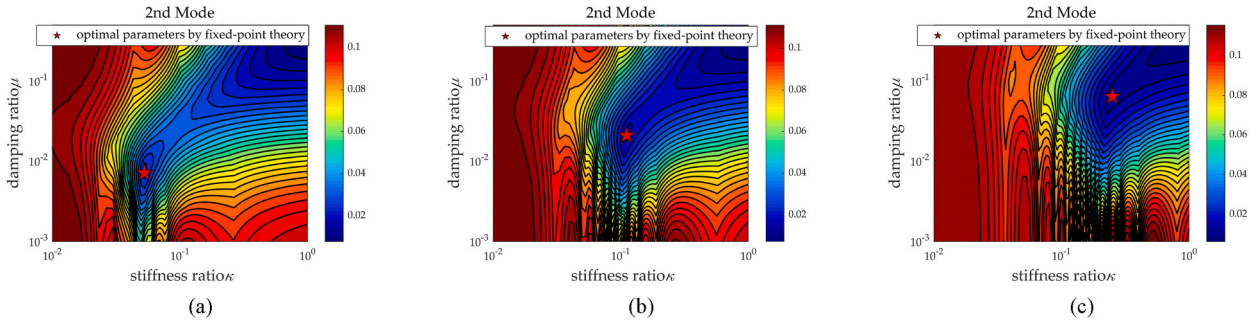

Fig. 19. Contour plots of the maximum displacement response of the structural second mode equivalent system(a) $\mu = 0.05$;(b) $\mu = 0.10$;(c) $\mu = 0.20$.

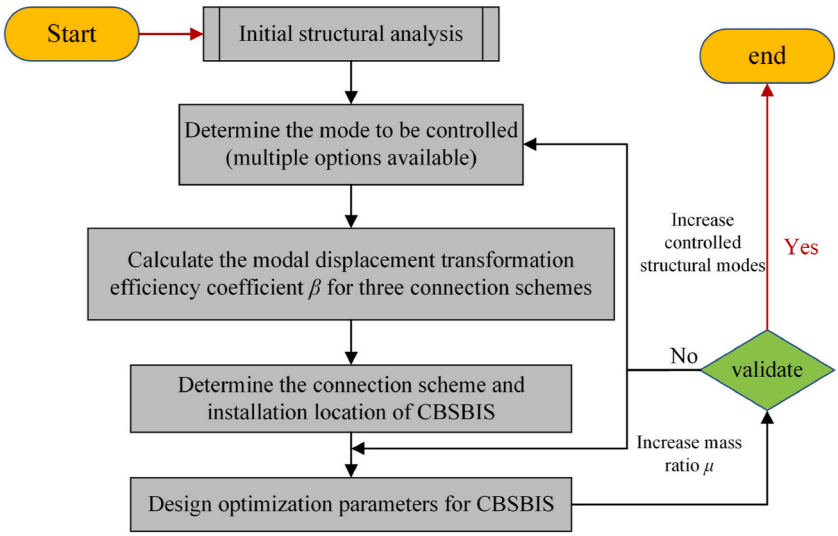

Fig. 20. Design flowchart of the CBSBIS.

4. Case validation and comparison

This section selects a total of 24 natural seismic waves in accordance with Chinese code [62], including pulse-like and no pulse-like seismic waves as inputs to verify the optimization effect of different cable-bracing schemes and locations of CBSBIS on the control of structural dynamic response. Meanwhile, the performance of CBSBIS is also compared with two different damping systems, a damped outrigger (DO) with the same additional damping parameters and a tuned mass damper (TMD) with the same mass. It is reasonable to posit that the true physical mass of the TMD and the CBSBIS is equivalent in the comparison, given that both the TMD and the CBSBIS function by being tuned to a specific frequency. An important metric of a tuned damping system is the additional mass required. Note that it is assumed that the apparent mass amplification of the CBSBIS is 100 times, which means that the mass of the TMD is 1/100 of the apparent mass of the CBSBIS. The parameters of the TMD are optimally designed using fixed point theory method described in Ref. [63] which is the same optimization as the CBSBIS. Fig. 21 shows a schematic diagram of the TMD attached to the top of the structure. Also, in a conventional damped outrigger structure, the other end of the damper is attached to the perimeter column and therefore the axial deformation of the perimeter column has to be taken into account. The analysis in this paper is simplified by the fact that the perimeter column is considered to have infinite stiffness. The damped outrigger (DO) structure is shown in Fig. 22. This simplification takes too much account of the role of dampers.

For the first-order modal control of the structure, it is assumed that the CBSBIS is installed in different cable-bracing schemes, with their respective modal generalized mass ratios of 0.05. At the same time, the first and second order modes are considered to be controlled simultaneously for the vertical cable-bracing scheme, and compared with the different damping systems. The parameters of the CBSBIS for different topological forms and damping system are shown in Table 3. Strategies 1–4 correspond to different topological forms of CBSBIS and 5–6 correspond to different damping systems.

To better quantify and compare the control effects of different systems on the dynamic response of the frame-core tube structure, two indicators, the floor acceleration and the harmful inter-story drift ratio, are selected as control objects. The harmful inter-story drift ratio is defined as follows:

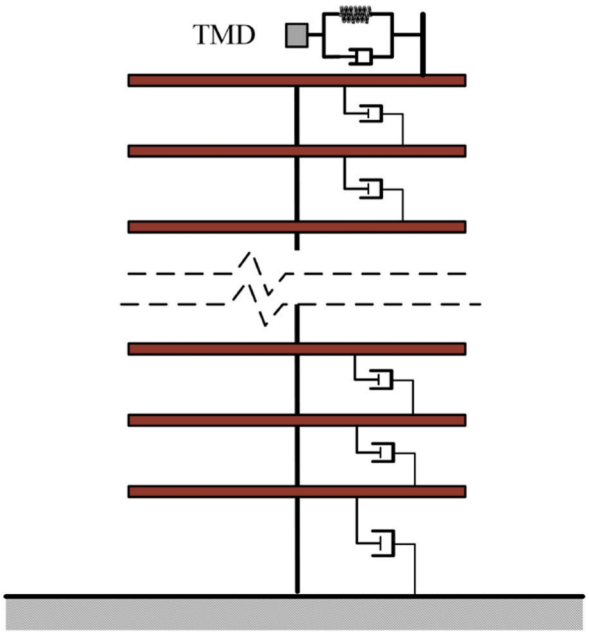

Fig. 21. A TMD attached to the top of the structure.

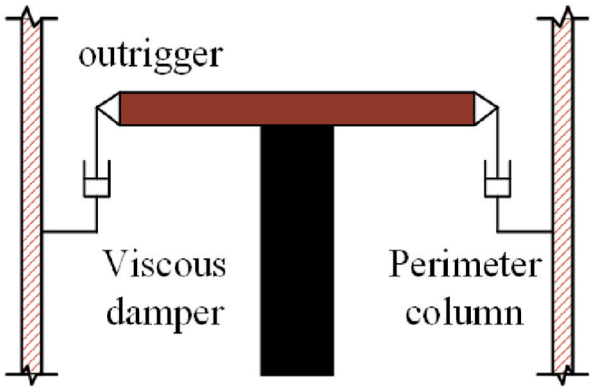

Fig. 22. Damped outrigger structure.

$$\Delta_j = \frac{x_j - x_{j-1} - \theta_{j-1} h_{j-1}}{h_{j-1}} \tag{27}$$

where Δ_j is the harmful inter-story drift ratio of layer j, x_j is the displacement of layer j, and θ_j is the rotation angle of layer j. The harmful inter-story drift ratio is more representative of the deformation state of the structure than the traditional definition of inter-story drift ratio, as it neglects the difference in floor displacement due to rotation of the rigid body. At the same time, for a more intuitive representation of the performances of different vibration control systems and topology optimization, the acceleration control ratios γ_a and the harmful inter-story drift ratio control ratios γ_Δ are defined as follows：

Table 3
Specific parameters for different topological forms of CBSBIS and damping systems.

Strategy			installation position	$m_d(10^7 kg)$	$k_d(10^8 N/m)$	$c_d(10^7 N/m/s)$
1	CBSBIS	Vertical bracing	(0,40)	0.65	0.39	0.44
2			(0,40), (9,40)	0.65,0.055	0.39,1.26	0.44,0.23
3		Inverted-V bracing	(0,40)	1.26	0.76	0.86
4		Diagonal bracing	(0,40)	3.41	2.05	2.32
5	DO		(39,40)	–	∞	0.67
6	TMD		40	$0.71e^{-2}$	$3.79e^{-3}$	$3.55\ e^{-3}$

$$\begin{cases} \gamma_a = \dfrac{a_0 - a}{a_0} \\ \gamma_\Delta = \dfrac{\Delta_0 - \Delta}{\Delta_0} \end{cases} \tag{28}$$

where a and Δ are the controlled structural acceleration and harmful inter-story drift ratio; a_0 and Δ_0 are the uncontrolled structural acceleration and harmful inter-story drift ratio.

Fig. 23 shows the mean and max control ratios of the structure equipped with different topological forms of CBSBIS for the mean square value of the acceleration at the top of the structure and the maximum value of the harmful inter-story drift ratio at the bottom under multiple seismic waves inputs. Fig. 25 shows the maximum dynamic response of the structure at each floor for one of the seismic wave inputs. It is evident that the control performance of the three cable-bracing schemes is similar for the same modal generalized mass ratio. However, the vertical bracing scheme requires smaller optimization parameters than the other two, indicating more efficient control. Furthermore, the additional mass required by CBSBIS for the three connection schemes is in agreement with the ratio of the calculated modal displacement transformation efficiency coefficient β. This corroborates the findings of the previous sections, which indicate that the vertical bracing scheme is more effective in utilizing the overall bending deformation of the frame-core tube structure, particularly through the outriggers, which amplify the displacement driving the CBSBIS. Comparison of strategies 1 and 2 reveals that simultaneous control of multiple modes of the structure gives better results. It is evident that strategy 2 is significantly more effective than strategy 1 for acceleration control, possibly because the higher order modes of the structure contribute more to the acceleration. Therefore, in practice, multiple modes can be selected for simultaneous control. Figs. 24 and 26 compare the performance of CBSBIS with two other damping systems. It can be observed that CBSBIS outperforms the remaining two vibration damping systems, both in terms of structural harmful inter-story drift ratio and top floor acceleration control. In particular, CBSBIS can demonstrate a thousandfold amplification through rational design, which has a significant effect on the lightweighting of high-rise or ultra-high-rise vibration damping systems. Fig. 27 illustrates the acceleration time history at the top of the structure for a specific seismic wave input, which provides a more detailed visual representation of the control effect of the CBSBIS. The force-displacement curve of the damper in Fig. 28 shows the more efficient energy consumption of the CBSBIS. The CBSBIS damped hysteresis loop is fuller which means more energy dissipated than the damped outrigger.

5. Conclusions

This article explains the fundamentals of the self-balanced inerter and how it may be used in cable-bracing systems. It also suggests various cable connection schemes and goes into considerable detail about how to calculate the cable's displacement while using each method. Based on the motion equations of the different connection schemes applied to the frame-core tube structure, the optimal design methods and topological analysis of the CBSBIS are proposed. And an example is used to validate the accuracy of the analysis. The damping energy dissipation and control effects of CBSBIS and two other damping systems are verified by comparison with examples. The main conclusions are as follows.

(1) The self-balanced inerter can realize the self-balanced of the torque on the lead screw by adopting the design method of lead screw with right-hand and left-hand threads, which is convenient for the application of the pure tension system and obtains thousands of times magnification of apparent mass.

(2) The cable-bracing schemes and installation positions of the CBSBIS system in the frame-core tube structure significantly affect its control effect. The vertical bracing scheme is more effective in utilizing the overall bending deformation of the frame-core tube structure, particularly through the outriggers, which amplify the displacement driving the CBSBIS. The vertical bracing scheme in the example structure is highly efficient in utilizing structural deformation, with a capacity to accommodate deformation of up to 100 % and 400 % greater than that of inverted-V bracing and diagonal bracing schemes, respectively. The

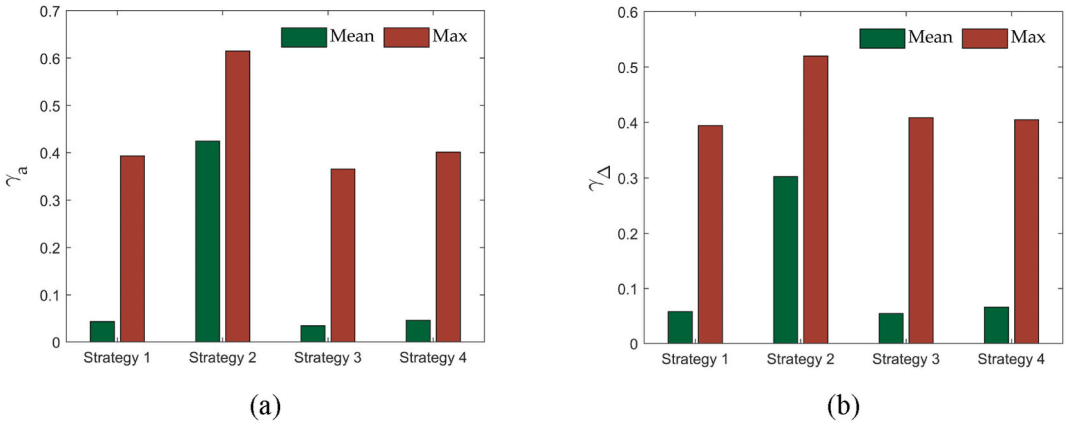

Fig. 23. Control ratios of different topological forms of CBSBIS (a) γ_a for top layer; (b) γ_Δ for bottom.

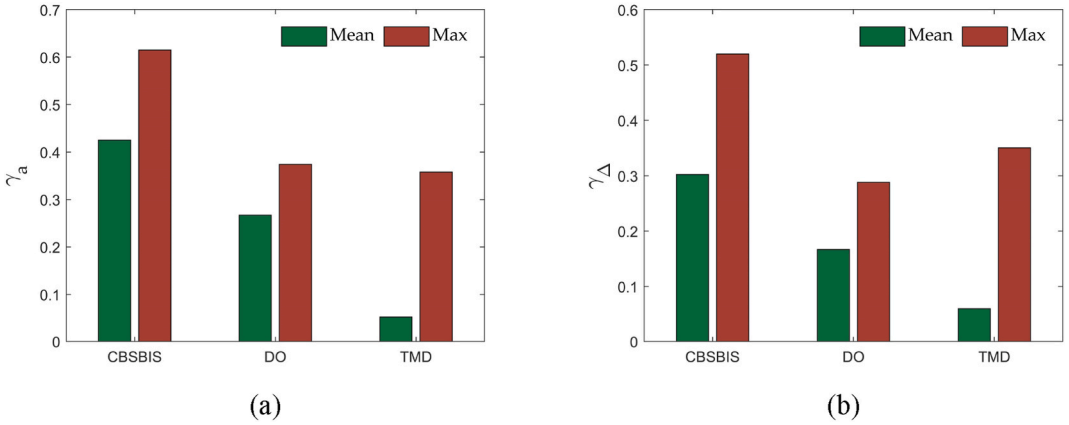

Fig. 24. Control ratios of different damping systems (a) γ_a for top layer; (b) γ_Δ for bottom.

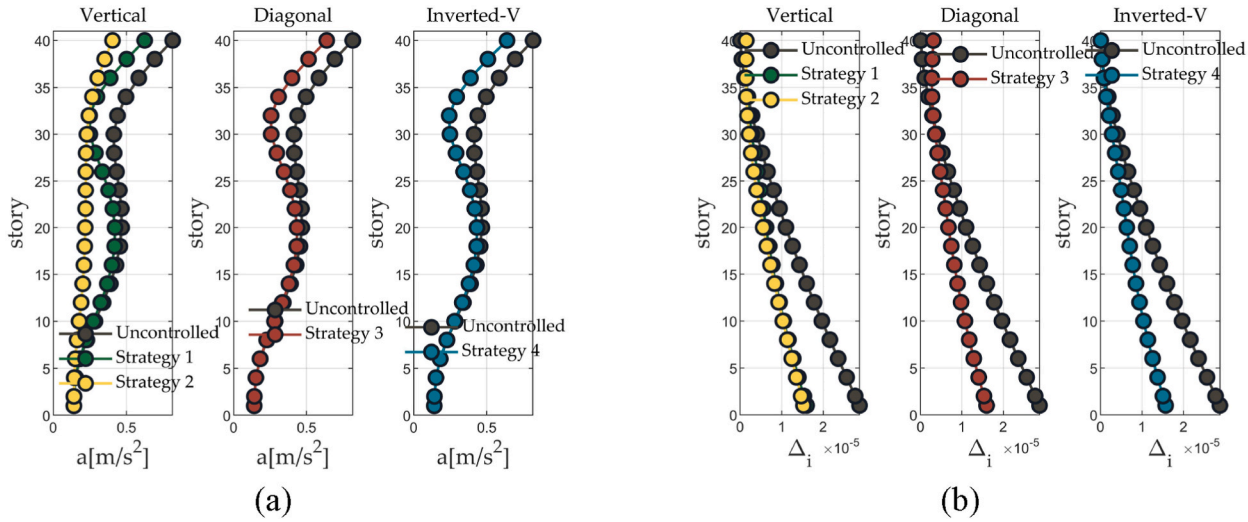

Fig. 25. Maximum dynamic response of CBSBIS for different topological forms under CHICHI seismic wave (a) floor acceleration; (b) harmful inter-story drift ratio.

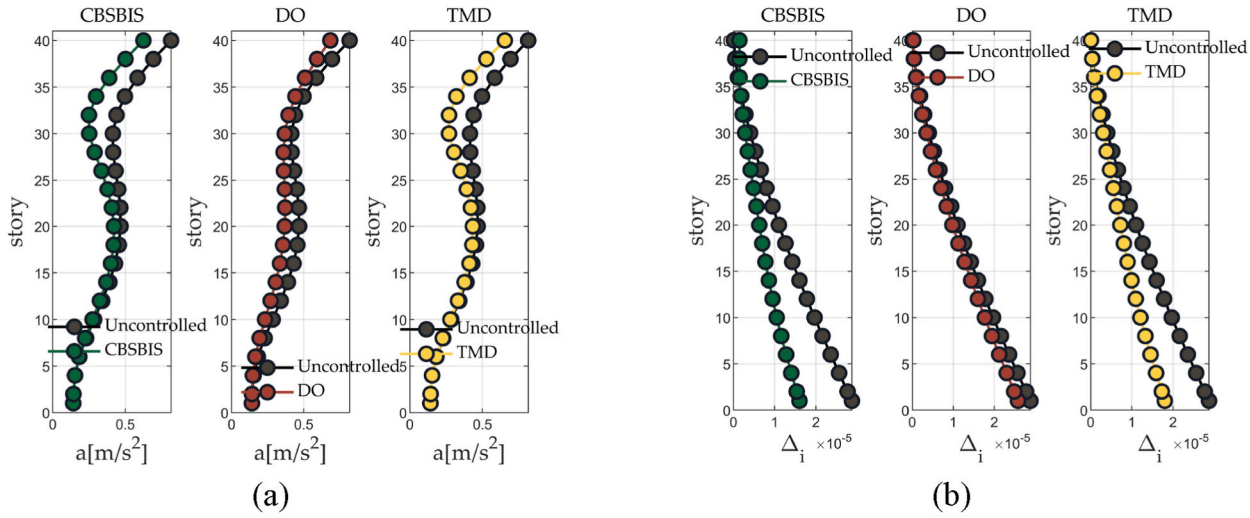

Fig. 26. Maximum dynamic response of different damping systems under CHICHI seismic wave (a) floor acceleration; (b) harmful inter-story drift ratio.

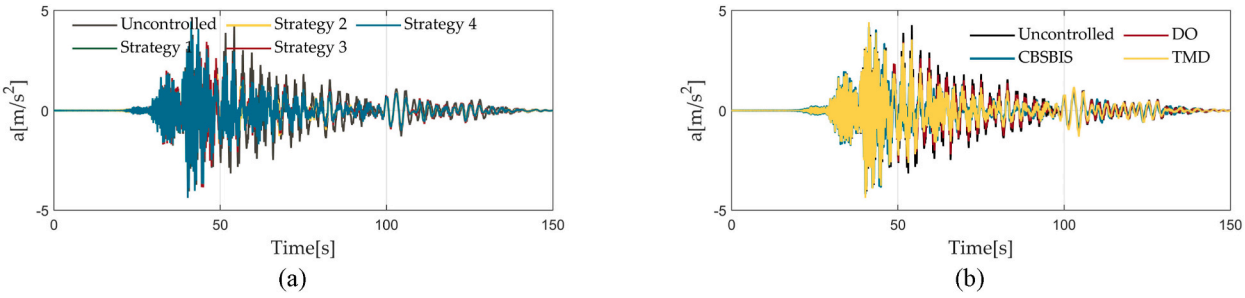

Fig. 27. Example of top acceleration time history (a) topology optimization comparison; (b) different damping systems comparison.

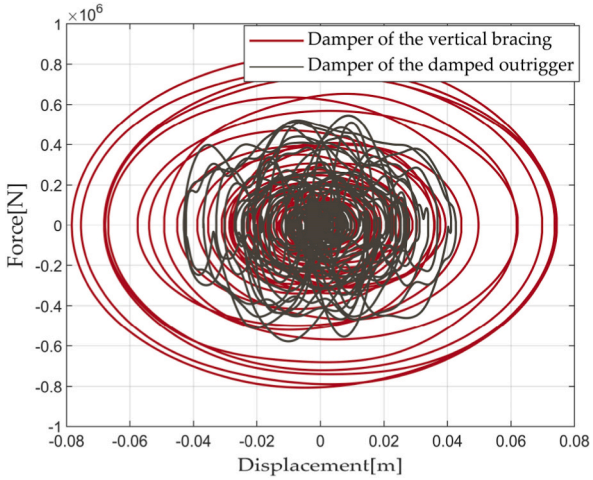

Fig. 28. Comparison of the force-displacement curves of the damper for the CBSBIS and damped outrigger.

method of structural modal control can select the installation position of CBSBIS more rationally and make the design of CBSBIS simpler.

(3) The frame-core tube structure equipped with CBSBIS for topology optimization and modal control has significantly improved the control of the structure's harmful inter-story drift ratio and acceleration response through the time-history analysis of multiple seismic waves. Specifically, the simultaneous control of the first two modes of the structure in the example analysis yields an average improvement of 57 % in the acceleration control ratio γ_a and an average improvement of 32 % in the harmful inter-story drift ratio control ratios γ_Δ, in comparison to controlling the first mode of the structure. Compared to the traditional damped outrigger control system and TMD, CBSBIS demonstrates more efficient energy consumption and control performance which improves the γ_a and γ_Δ of the structure by an average of 65 % and 81 % compared to the DO, and an average of 72 % and 48 % compared to the TMD.

Of course, it is evident that CBSBIS possesses certain inherent limitations in practical engineering applications. For instance, the cross-floor cable arrangement exerts a pronounced influence on the original building layout of the structure, and the efficiency of the cable displacement conversion is diminished in the non-outrigger structure. Consequently, the actual CBSBIS topology optimization results must be enhanced by integrating project situation-specific considerations, such as utilizing existing lift shafts, pipelines and other available spaces to arrange the cable in a manner that avoids the necessity for additional openings or a greater impact on the building layout.

CRediT authorship contribution statement

Liyu Xie: Writing – review & editing, Supervision, Methodology, Investigation, Funding acquisition, Conceptualization. **Zijian Yang:** Writing – review & editing, Writing – original draft, Visualization, Validation, Software, Methodology, Investigation, Formal analysis, Conceptualization. **Songtao Xue:** Supervision, Resources, Methodology, Investigation, Funding acquisition, Conceptualization. **Ling Gong:** Writing – original draft, Visualization, Validation, Software, Methodology, Formal analysis, Conceptualization. **Hesheng Tang:** Writing – review & editing, Supervision, Resources, Methodology, Investigation, Conceptualization.

Declaration of competing interest

The authors declare that they have no known competing financial interests or personal relationships that could have appeared to influence the work reported in this paper.

Data availability

Data will be made available on request.

Acknowledgements

The authors would like to acknowledge the support of the National Key R&D Program of China (2021YFE0112200) and Natural Science Foundation of Shanghai (20ZR1461800).

References

[1] W. Alhaddad, Y. Halabi, H. Xu, H. Lei, A comprehensive introduction to outrigger and belt-truss system in skyscrapers, Structures 27 (2020) 989–998, https://doi.org/10.1016/j.istruc.2020.06.028.
[2] P.S. Kian, The use of outrigger and belt truss system for high-rise concrete buildings, Civil Engineering Dimension 3 (2001) 36–41. https://ced.petra.ac.id/index.php/civ/article/view/15536/15528.
[3] J. Hoenderkamp, M. Bakker, Analysis of highrise braced frames with outriggers, Struct. Des. Tall Special Build. 12 (2003) 335–350, https://doi.org/10.1002/tal.226.
[4] S. Lee, A. Tovar, Outrigger placement in tall buildings using topology optimization, Eng. Struct. 74 (2014) 122–129, https://doi.org/10.1016/j.engstruct.2014.05.019.
[5] H.-S. Kim, Y.-J. Lim, H.-L. Lee, Optimum location of outrigger in tall buildings using finite element analysis and gradient-based optimization method, J. Build. Eng. 31 (2020) 101379, https://doi.org/10.1016/j.jobe.2020.101379.
[6] N. Satake, K.-i. Suda, T. Arakawa, A. Sasaki, Y. Tamura, Damping evaluation using full-scale data of buildings in Japan, J. Struct. Eng. 129 (2003) 470–477, https://doi.org/10.1061/(asce)0733-9445(2003)129:4(470.
[7] R. Smith, R. Merello, M. Willford, Intrinsic and supplementary damping in tall buildings, Proceedings of the Institution of Civil Engineers - Structures and Buildings 163 (2010) 111–118, https://doi.org/10.1680/stbu.2010.163.2.111.
[8] L. Xing, P. Gardoni, Y. Zhou, M. Aguaguiña, Optimal outrigger locations and damping parameters for single-outrigger systems considering earthquake and wind excitations, Eng. Struct. 245 (2021) 112868, https://doi.org/10.1016/j.engstruct.2021.112868.
[9] Y. Zhou, L. Xing, Seismic performance evaluation of a viscous damper-outrigger system based on response spectrum analysis, Soil Dynam. Earthq. Eng. 142 (2021) 106553, https://doi.org/10.1016/j.soildyn.2020.106553.
[10] R.J. Smith, M.R. Willford, The damped outrigger concept for tall buildings, Struct. Des. Tall Special Build. 16 (2007) 501–517, https://doi.org/10.1002/tal.413.
[11] Y. Zhou, C. Zhang, X. Lu, Seismic performance of a damping outrigger system for tall buildings, Struct. Control Health Monit. 24 (2017) e1864, https://doi.org/10.1002/stc.1864.
[12] P. Tan, C. Fang, C. Chang, B. Spencer, F. Zhou, Dynamic characteristics of novel energy dissipation systems with damped outriggers, Eng. Struct. 98 (2015) 128–140, https://doi.org/10.1016/j.engstruct.2015.04.033.
[13] P. Tan, C. Fang, F. Zhou, Dynamic characteristics of a novel damped outrigger system, Earthq. Eng. Eng. Vib. 13 (2014) 293–304, https://doi.org/10.1007/s11803-014-0231-3.
[14] S. Das, S. Tesfamariam, Multiobjective design optimization of multi-outrigger tall-timber building: using SMA-based damper and Lagrangian model, J. Build. Eng. 51 (2022) 104358, https://doi.org/10.1016/j.jobe.2022.104358.
[15] S. Das, S. Tesfamariam, Optimization of SMA based damped outrigger structure under uncertainty, Eng. Struct. 222 (2020) 111074, https://doi.org/10.1016/j.engstruct.2020.111074.
[16] M. Wang, S. Nagarajaiah, F.-F. Sun, Dynamic characteristics and responses of damped outrigger tall buildings using negative stiffness, J. Struct. Eng. 146 (2020) 04020273, https://doi.org/10.1061/(asce)st.1943-541x.0002846.
[17] F.-F. Sun, M. Wang, S. Nagarajaiah, Multi-objective optimal design and seismic performance of negative stiffness damped outrigger structures considering damping cost, Eng. Struct. 229 (2021) 111615, https://doi.org/10.1016/j.engstruct.2020.111615.
[18] Z. Wang, Y. Zhou, C. Fang, J. Zhang, Stochastic optimization and sensitivity analysis of the combined negative stiffness damped outrigger and conventional damped outrigger systems subjected to nonstationary seismic excitation, Struct. Control Health Monit. 2023 (2023) 4024741, https://doi.org/10.1155/2023/4024741.
[19] R. Rana, T. Soong, Parametric study and simplified design of tuned mass dampers, Eng. Struct. 20 (1998) 193–204, https://doi.org/10.1016/s0141-0296(97)00078-3.
[20] S. Elias, V. Matsagar, Research developments in vibration control of structures using passive tuned mass dampers, Annu. Rev. Control 44 (2017) 129–156, https://doi.org/10.1016/j.arcontrol.2017.09.015.
[21] F. Yang, R. Sedaghati, E. Esmailzadeh, Vibration suppression of structures using tuned mass damper technology: a state-of-the-art review, J. Vib. Control 28 (2022) 812–836, https://doi.org/10.1177/1077546320984305.
[22] M.C. Smith, Synthesis of mechanical networks: the inerter, IEEE Trans. Automat. Control 47 (2002) 1648–1662.
[23] K. Ikago, K. Saito, N. Inoue, Optimum multi-modal seismic control design of high-rise buildings using tuned viscous mass dampers, in: Proceedings of the 13th International Conference on Civil, Structural and Environmental Engineering Computing Stirlingshire, Scotlan, Civil Comp Press, 2011, https://doi.org/10.4203/ccp.96.170. Paper 170.
[24] K. Ikago, K. Saito, N. Inoue, Seismic control of single-degree-of-freedom structure using tuned viscous mass damper, Earthq. Eng. Struct. Dynam. 41 (2012) 453–474, https://doi.org/10.1002/eqe.1138.
[25] K. Ikago, Y. Sugimura, K. Saito, N. Inoue, Optimum seismic response control of multiple degree of freedom structures using tuned viscous mass dampers, in: Proceedings of The10th International Conference on Computational Structures Technology, Stirlingshire, Scotland, Civil Comp Press, 2010, https://doi.org/10.4203/ccp.93.164. Paper 164.
[26] K. Ikago, Y. Sugimura, K. Saito, N. Inoue, Seismic displacement control of multiple-degree-of-freedom structures using tuned viscous mass dampers, in: Proceedings of the 8th International Conference on Structural Dynamics, EURODYN, Leuven, Belgium, 2011.
[27] K. Ikago, Y. Sugimura, K. Saito, N. Inoue, Simple design method for a tuned viscous mass damper seismic control system, in: Proceedings of the 15th World Conference on Earthquake Engineering, 2012. Lisbon, Portugal.
[28] I.F. Lazar, S.A. Neild, D.J. Wagg, Using an inerter-based device for structural vibration suppression, Earthq. Eng. Struct. Dynam. 43 (2014) 1129–1147, https://doi.org/10.1002/eqe.2390.
[29] I.F. Lazar, S.A. Neild, D.J. Wagg, Vibration suppression of cables using tuned inerter dampers, Eng. Struct. 122 (2016) 62–71, https://doi.org/10.1016/j.engstruct.2016.04.017.

[30] L. Marian, A. Giaralis, Optimal design of a novel tuned mass-damper–inerter (TMDI) passive vibration control configuration for stochastically support-excited structural systems, Probabilist. Eng. Mech. 38 (2014) 156–164, https://doi.org/10.1016/j.probengmech.2014.03.007.
[31] D. Patsialis, A. Taflanidis, A. Giaralis, Tuned-mass-damper-inerter optimal design and performance assessment for multi-storey hysteretic buildings under seismic excitation, Bull. Earthq. Eng. 21 (2023) 1541–1576, https://doi.org/10.1007/s10518-021-01236-4.
[32] J. Kang, S. Xue, L. Xie, H. Tang, R. Zhang, Multi-modal seismic control design for multi-storey buildings using cross-layer installed cable-bracing inerter systems: Part 1 theoretical treatment, Soil Dynam. Earthq. Eng. 164 (2023) 107639, https://doi.org/10.1016/j.soildyn.2022.107639.
[33] R. Jia, X. Ji, Y. Cheng, K. Ikago, Seismic response control of core wall structures using tuned viscous mass damper (TVMD) outriggers, Eng. Struct. 292 (2023) 116546, https://doi.org/10.1016/j.engstruct.2023.116546.
[34] S. Djerouni, A. Ounis, S. Elias, M. Abdeddaim, R. Rupakhety, Optimization and performance assessment of tuned mass damper inerter systems for control of buildings subjected to pulse-like ground motions, in: Structures, Elsevier, 2022, https://doi.org/10.1016/j.istruc.2022.02.007.
[35] X. Shi, W. Shi, K. Lin, L. Xing, S. Zhu, Optimal design of tuned inerter dampers with series or parallel stiffness connection for cable vibration control, Struct. Control Health Monit. 28 (2021) e2673, https://doi.org/10.1002/stc.2673.
[36] S. Djerouni, M. Abdeddaim, S. Elias, R. Rupakhety, Optimum double mass tuned damper inerter for control of structure subjected to ground motions, J. Build. Eng. 44 (2021) 103259, https://doi.org/10.1016/j.jobe.2021.103259.
[37] D. Pietrosanti, M. De Angelis, A. Giaralis, Experimental study and numerical modeling of nonlinear dynamic response of SDOF system equipped with tuned mass damper inerter (TMDI) tested on shaking table under harmonic excitation, Int. J. Mech. Sci. 184 (2020) 105762, https://doi.org/10.1016/j.ijmecsci.2020.105762.
[38] L. Cao, C. Li, X. Chen, Performance of multiple tuned mass dampers-inerters for structures under harmonic ground acceleration, Smart Structures and Systems, Int. J. 26 (2020) 49–61, https://doi.org/10.12989/sss.2020.26.1.049.
[39] J. Dai, Z.-D. Xu, P.-P. Gai, Tuned mass-damper-inerter control of wind-induced vibration of flexible structures based on inerter location, Eng. Struct. 199 (2019) 109585, https://doi.org/10.1016/j.engstruct.2019.109585.
[40] C. Pan, R. Zhang, Design of structure with inerter system based on stochastic response mitigation ratio, Struct. Control Health Monit. 25 (2018) e2169, https://doi.org/10.1002/stc.2169.
[41] S. Elias, M. Beer, Vibration control and energy harvesting of offshore wind turbines installed with TMDI under dynamical loading, Eng. Struct. 315 (2024) 118459, https://doi.org/10.1016/j.engstruct.2024.118459.
[42] G. Alotta, C. Biondo, A. Giaralis, G. Failla, Seismic protection of land-based wind turbine towers using the tuned inerter damper, in: Structures, Elsevier, 2023, https://doi.org/10.1016/j.istruc.2023.03.004.
[43] D. Ning, S. Sun, H. Du, W. Li, N. Zhang, M. Zheng, L. Luo, An electromagnetic variable inertance device for seat suspension vibration control, Mech. Syst. Signal Process. 133 (2019) 106259, https://doi.org/10.1016/j.ymssp.2019.106259.
[44] Y. Hu, M.Z. Chen, Z. Shu, Passive vehicle suspensions employing inerters with multiple performance requirements, J. Sound Vib. 333 (2014) 2212–2225, https://doi.org/10.1016/j.jsv.2013.12.016.
[45] X. Dong, Y. Liu, M.Z. Chen, Application of inerter to aircraft landing gear suspension, in: 2015 34th Chinese Control Conference (CCC), IEEE, 2015.
[46] K. Sugiura, R. Sawada, Y. Nemoto, R. Haraguchi, T. Asai, Wave flume testing of an oscillating-body wave energy converter with a tuned inerter, Appl. Ocean Res. 98 (2020) 102127, https://doi.org/10.1016/j.apor.2020.102127.
[47] N.U. Islam, R. Jangid, Optimum parameters of tuned inerter damper for damped structures, J. Sound Vib. 537 (2022) 117218, https://doi.org/10.1016/j.jsv.2022.117218.
[48] C. Pan, R. Zhang, H. Luo, C. Li, H. Shen, Demand-based optimal design of oscillator with parallel-layout viscous inerter damper, Struct. Control Health Monit. 25 (2018) e2051, https://doi.org/10.1002/stc.2051.
[49] R. Zhang, Z. Zhao, C. Pan, K. Ikago, S. Xue, Damping enhancement principle of inerter system, Struct. Control Health Monit. 27 (2020) e2523, https://doi.org/10.1002/stc.2523.
[50] Y. Peng, P. Sun, Reliability-based design optimization of tuned mass-damper-inerter for mitigating structural vibration, J. Sound Vib. 572 (2024) 118166, https://doi.org/10.1016/j.jsv.2023.118166.
[51] T. Asai, K. Ikago, Y. Araki, Outrigger tuned viscous mass damping system for high-rise buildings subject to earthquake loadings, in: Proceedings of the 6th International Conference on Advances in Experimental Structural Engineering, University of Illinois, Urbana-Champaign, United States, 2015.
[52] T. Asai, Y. Watanabe, Outrigger tuned inertial mass electromagnetic transducers for high-rise buildings subject to long period earthquakes, Eng. Struct. 153 (2017) 404–410, https://doi.org/10.1016/j.engstruct.2017.10.040.
[53] L. Xie, X. Ban, S. Xue, K. Ikago, J. Kang, H. Tang, Theoretical study on a cable-bracing inerter system for seismic mitigation, Appl. Sci. 9 (2019) 4096, https://doi.org/10.3390/app9194096.
[54] S. Xue, J. Kang, L. Xie, R. Zhang, X. Ban, Cross-layer installed cable-bracing inerter system for MDOF structure seismic response control, Appl. Sci. 10 (2020) 5914, https://doi.org/10.3390/app10175914.
[55] G. Pekcan, Design of Seismic Energy Dissipation Systems for Reinforced Concrete and Steel Structures, State University of New York at Buffalo, 1998.
[56] X. Hou, H. Tagawa, Displacement-restraint bracing for seismic retrofit of steel moment frames, J. Constr. Steel Res. 65 (2009) 1096–1104, https://doi.org/10.1016/j.jcsr.2008.11.008.
[57] N. Gao, J.-S. Jeon, D.E. Hodgson, R. DesRoches, An innovative seismic bracing system based on a superelastic shape memory alloy ring, Smart Mater. Struct. 25 (2016) 055030, https://doi.org/10.1088/0964-1726/25/5/055030.
[58] A. Falahian, P. Asadi, H. Tajmir Riahi, M. Kadkhodaei, An experimental study on a self-centering damper based on shape-memory alloy wires, Mech. Base. Des. Struct. Mach. 51 (2023) 3779–3802, https://doi.org/10.1080/15397734.2021.1939048.
[59] C.S. Lee, J.-S. Jeon, Seismic risk-based optimization of tension-only shape-memory alloy device for steel moment-resisting frames, Eng. Struct. 296 (2023) 116976, https://doi.org/10.1016/j.engstruct.2023.116976.
[60] J.-D. Kang, H. Tagawa, Seismic performance of steel structures with seesaw energy dissipation system using fluid viscous dampers, Eng. Struct. 56 (2013) 431–442, https://doi.org/10.1016/j.engstruct.2013.05.015.
[61] R. Gamaliel, Frequency-based Response of Damped Outrigger Systems for Tall Buildings, Massachusetts Institute of Technology, 2008. Ph.D. thesis.
[62] GB50011–2010, Code for Seismic Design of Buildings, China Architecture & Building Press: Ministry of Housing and Urban-Rural Development of the People's Republic of China, Beijing, 2010.
[63] J.P. Den Hartog, Mechanical vibrations, Courier Corporation (1985).